

Supersolid gap soliton in a Bose-Einstein condensate and optical ring cavity coupling systemJieli Qin ^{*}*School of Physics and Materials Science, Guangzhou University, 230 Wai Huan Xi Road,
Guangzhou Higher Education Mega Center, Guangzhou 510006, China*Lu Zhou [†]*Department of Physics, School of Physics and Electronic Science, East China Normal University, Shanghai 200241, China
and Collaborative Innovation Center of Extreme Optics, Shanxi University, Taiyuan, Shanxi 030006, China*

(Received 17 February 2022; accepted 15 May 2022; published 31 May 2022)

The system of a transversely pumped Bose-Einstein condensate (BEC) coupled to a lossy ring cavity can favor a supersolid steady state. Here we find the existence of supersolid gap soliton in such a driven-dissipative system. By numerically solving the mean-field atom-cavity field coupling equations, gap solitons of a few different families have been identified. Their dynamical properties, including stability, propagation, and soliton collision, are also studied. Due to the feedback atom-intracavity field interaction, these supersolid gap solitons show numerous new features compared with the usual BEC gap solitons in static optical lattices.

DOI: [10.1103/PhysRevE.105.054214](https://doi.org/10.1103/PhysRevE.105.054214)**I. INTRODUCTION**

Due to the effect of dispersion, a wave packet would suffer a spatial spreading during its time evolution. However, when there also exists appropriate nonlinearity in the system, the dispersion spreading can be suppressed and give rise to a nonspreading localized wave packet—soliton [1]. In a Bose-Einstein condensate (BEC) system, the nonlinearity due to attractive interatom contact interaction can well balance the dispersion spreading and support a matter wave soliton, which is particularly called a “bright soliton” [2–8]. While for the repulsive interaction, instead of a nonspreading wave packet, it only supports a localized atomic density dip (i.e., absence of atoms) on the background BEC density profile, which is usually named as dark soliton [9–15] (these solitons are originally studied in the field of nonlinear optics, so according to the brightness of the light pulses, they are described by the words “bright” and “dark” [16–18]). When BEC is loaded into a periodical optical lattice potential, its dispersion property can be substantially changed, as a result, even for the repulsive interaction there can also exist a bright soliton. Since the chemical potential of such a soliton falls into the energy gaps of the optical lattice potential, it is given the name of gap soliton [19–39]. In passing, we also mention that although gap solitons usually refer to the bright ones, there do exist dark gap solitons [40–43] which are not the concerns of this paper.

Supersolid is an unusual state of matter that simultaneously behaves as both a crystalline solid and a superfluid [44–48]. Originally, it was predicted for helium as early as the middle of the 20th Century [49–53], but until now it still has

not been observed undoubtedly [54–58]. In recent years, the highly controllable atomic quantum gas brings new vitality to the supersolid studies. It has been experimentally realized in several different types of systems. The ground state of a spin-orbit coupled BEC can fall into a stripe phase exhibiting supersolid properties [59–61]. In dipolar BEC, the balance between long range dipole-dipole interaction and short range contact interaction gives rise to the emergence of arrays of quantum droplets, i.e., dipolar supersolid [62–68]. The cavity-mediated interaction also can lead to BEC supersolid. Two different schemes have already been experimentally reported, one of them couples the BEC to two crossed linear optical cavities [69,70], while the other one uses a ring cavity [71,72].

In this work, we are interested in the driven-dissipative supersolid BEC realized by the ring cavity scheme, for details of the physical model see Sec. II or the original paper [71]. In this scheme, the BEC collectively scatters the pumping photons into the cavity, and results in a super-radiant optical lattice, which backwardly drives the BEC into a supersolid state. As having been pointed out in the first paragraph of this section, the simultaneous existence of an optical lattice and interaction nonlinearity would lead to gap solitons in BEC. In this vein of thought, we propose that there would exist supersolid gap solitons in a BEC and ring cavity coupling system. The main objectives of this work are finding out such soliton solutions, and studying their basic properties.

The rest contents of this paper are organized as follows: In Sec. II, we briefly describe the considering system, and present the theoretical formulas to handle its steady state and dynamical evolution. The next Sec. III shows the main results of this paper. It is split into four subsections, which deal with the gap soliton solutions (Sec. III A), their stability (Sec. III B), mobility (Sec. III C) and collision (Sec. III D) properties, respectively. At last, we summarize the paper in Sec. IV.

^{*}qinjeli@126.com; 104531@gzhu.edu.cn[†]lzhou@phy.ecnu.edu.cn

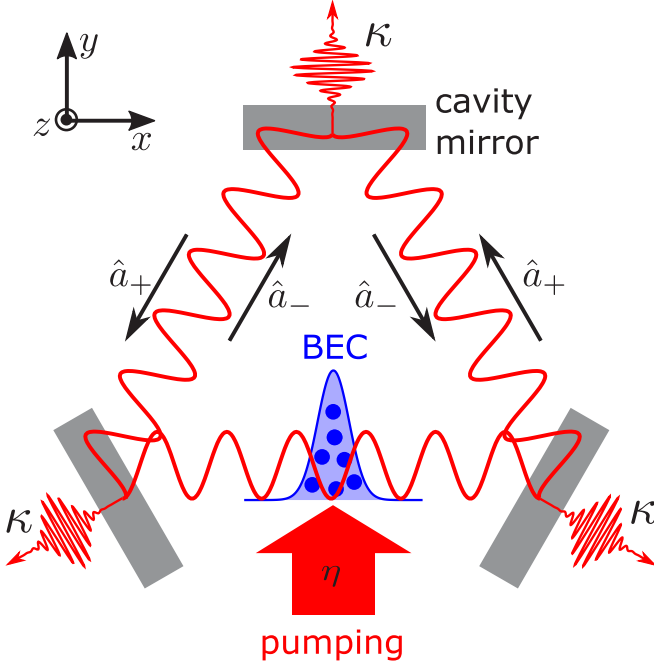


FIG. 1. Schematic diagram of the considering atomic BEC and optical ring cavity coupling system. A quasi-one-dimensional BEC is loaded in an optical ring cavity along its axis. By transversely pumping the BEC using a standing wave laser (pumping strength η), light fields are built up in the cavity due to super-radiant scattering of pumping photons into the two counterpropagating ring cavity optical modes ($\hat{a}_{\pm}e^{\pm ik_c x}$), and reach a steady state on account of the cavity loss (loss rate κ). Interference between lights of the two cavity modes forms an optical lattice. Backwardly, this optical lattice drives the BEC to a supersolid gap soliton state [71].

II. MODEL

As schematically shown in Fig. 1, in this work we consider an atomic BEC and optical ring cavity coupling system. The BEC is loaded in the ring cavity along the cavity axis, and is tightly trapped in the transverse (y, z) direction, such that only the longitudinal (x) direction dynamics need to be considered. When transversely illuminating a standing-wave laser on the BEC atoms (Rabi frequency Ω_0 and detuning Δ_a), light fields are built up in the cavity due to the scattering of pumping photons into the two counterpropagating ring cavity optical modes ($\hat{a}_{\pm}e^{\pm ik_c x}$ with \hat{a}_{\pm} being the annihilation operators and k_c being the wave number). Backwardly, the induced cavity light fields will also interact with the BEC atoms (strength \mathcal{G}_0). Such a system can be described by Hamiltonian [71]

$$\hat{H} = -\hbar\Delta_c(\hat{a}_+^\dagger\hat{a}_+ + \hat{a}_-^\dagger\hat{a}_-) + \int \hat{\psi}^\dagger(x)H_a\hat{\psi}(x)dx + \frac{1}{2} \int \hat{\psi}^\dagger(x)\hat{\psi}^\dagger(x')V(x-x')\hat{\psi}(x')\hat{\psi}(x)dx dx', \quad (1)$$

where \hbar is the Planck constant, Δ_c is the detuning between the cavity modes and pump laser, $\hat{\psi}$ is the field operator of the BEC. The first term describes the two counterpropagating cavity modes. The last term describes the interaction between BEC atoms. Considering the one-dimensional effective contact interaction [73], it is $V(x-x') = g\delta(x-x')$, where

$g = 2\hbar\omega_\perp a_s$ describes the interaction strength, with a_s being the s-wave scattering length, ω_\perp referring to the frequency of transverse confinement harmonic potential. When $g < 0$, it represents an attractive interaction, while for $g > 0$ it is a repulsive interaction. In this work, we consider the case of repulsive interaction. The middle term accounts for the kinetic and optical potential energy of the BEC, H_a is the corresponding single particle Hamiltonian

$$H_a = \frac{\hat{p}_x^2}{2m} + \hat{V}_{ac} + \hat{V}_{ap}, \quad (2)$$

with

$$\hat{V}_{ac} = \hbar U[\hat{a}_+^\dagger\hat{a}_+ + \hat{a}_-^\dagger\hat{a}_- + (\hat{a}_+^\dagger\hat{a}_-e^{-2ik_c x} + \text{H.c.})], \quad (3)$$

$$\hat{V}_{ap} = \hbar\eta(\hat{a}_+e^{ik_c x} + \hat{a}_-e^{-ik_c x} + \text{H.c.}). \quad (4)$$

Here, m is the atomic mass, $\hat{p}_x = -i\hbar\partial_x$ is the momentum operator along the x direction, hence $\hat{p}_x^2/(2m)$ is the kinetic energy term. The optical potential can be split into two parts. The part caused by two-photon scattering between the two cavity modes is denoted as \hat{V}_{ac} , its strength is $\hbar U = \hbar\mathcal{G}_0/\Delta_a$. The other part \hat{V}_{ap} is caused by two-photon scattering between pump and cavity modes, and its strength is $\hbar\eta = \hbar\mathcal{G}_0\Omega_0/\Delta_a$. In other words, this term describes the pumping of the system, so η would also be called an effective pumping strength. In the following contents, we will use the natural unit $m = \hbar = k_c = 1$ for simplicity of formulas.

Within the mean-field theory [74], the quantum operators are approximated by their mean values. The dynamical equations governing these mean-field variables can be obtained by taking mean values of the corresponding Heisenberg equations, and they are

$$i\frac{\partial}{\partial t}\alpha_{\pm} = (-\Delta_c + UN - i\kappa)\alpha_{\pm} + UN_{\pm 2}\alpha_{\mp} + \eta N_{\pm 1}, \quad (5)$$

$$i\frac{\partial}{\partial t}\psi = \left[-\frac{1}{2}\frac{\partial^2}{\partial x^2} + \mathcal{V}_{\text{eff}}(x)\right]\psi + |\psi|^2\psi, \quad (6)$$

with

$$N = \int |\psi(x)|^2 dx, \quad (7)$$

$$N_{\pm 1} = \int |\psi(x)|^2 e^{\mp ix} dx, \quad (8)$$

$$N_{\pm 2} = \int |\psi(x)|^2 e^{\mp 2ix} dx, \quad (9)$$

$$\mathcal{V}_{\text{eff}}(x) = \mathcal{V}_{ac}(x) + \mathcal{V}_{ap}(x), \quad (10)$$

$$\mathcal{V}_{ac} = U(|\alpha_+|^2 + |\alpha_-|^2) + U(\alpha_+^*\alpha_-e^{-2ix} + \text{c.c.}), \quad (11)$$

$$\mathcal{V}_{ap} = \eta(\alpha_+e^{ix} + \alpha_-e^{-ix} + \text{c.c.}), \quad (12)$$

being some auxiliary quantities to make the dynamical equations compact. Here, we have introduced the cavity loss with rate κ phenomenologically. And, we also have scaled the BEC wave function with the interatom interaction character length $l = \omega_\perp a_s m / (2\hbar k_c^2)$, $\psi \rightarrow \psi/\sqrt{l}$, therefore in Eq. (6) the coefficient before the nonlinear interaction term is simplified to 1. Under such a scaling, the normalization constant N should be interpreted as a scaled atom number. However, without

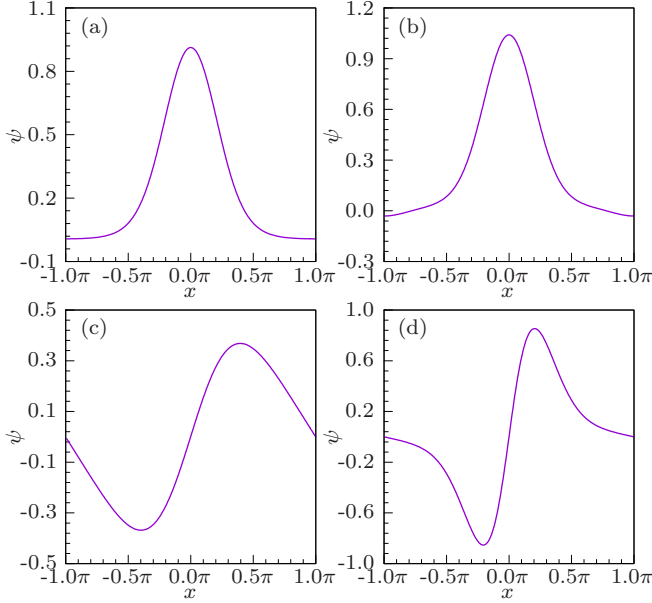


FIG. 2. Examples of spatially periodical supersolid states. Only one spatial period is considered here. Chemical potentials corresponding to these states are, respectively, $\mu = -3.10$ (a), -3.04 (b), 0.55 (c), and -1.31 (d), i.e., the same as those in Figs. 3(b) and 3(f), and Figs. 4(b) and 4(e). Parameters used are $\Delta_c = -1$, $U = -0.5$, $\kappa = 10$, $\eta = 15$ (this set of parameters will be used all along this paper).

leading to any misunderstanding, literally we will still call it “atom number” for convenience in the following contents.

Due to the balance between the pumping and cavity loss, the system will reach a steady state which can be mathematically obtained by letting $\partial_t \alpha_{\pm} = 0$, and $\psi(x, t) = \psi(x) e^{-i\mu t}$ with μ being the chemical potential. Inserting them into Eqs. (5) and (6), one gets the following time-independent equations for steady state

$$\mu \psi(x) = \left[-\frac{1}{2} \frac{\partial^2}{\partial x^2} + \mathcal{V}_{\text{eff}}(x) \right] \psi(x) + |\psi(x)|^2 \psi(x), \quad (13)$$

$$\alpha_+ = -\frac{(-\Delta_c + UN - i\kappa)\eta N_{+1} - \eta UN_{+2}N_{-1}}{(-\Delta_c + UN - i\kappa)^2 - U^2 N_{-2}N_{+2}}, \quad (14)$$

$$\alpha_- = -\frac{(-\Delta_c + UN - i\kappa)\eta N_{-1} - \eta UN_{-2}N_{+1}}{(-\Delta_c + UN - i\kappa)^2 - U^2 N_{-2}N_{+2}}. \quad (15)$$

We see that the BEC feels an optical lattice potential from the light fields. Since we are considering a running wave ring cavity, the location of this optical lattice is not predetermined by the cavity mirrors, and spontaneously breaks the continuous translation symmetry. This optical lattice will further modulate the BEC atomic density, that is, it will drive the BEC to a spatially periodical supersolid state [71,72]. For some examples of such states, one can see Fig. 2.

It is well known that when BEC with repulsive contact interaction is loaded in an optical lattice, even though the system is not well bounded, a kind of localized wave packet, i.e., gap soliton, can also exist due to the balance between repulsive interaction and anomalous dispersion [22]. Here, a supersolid optical lattice is also built up, thus we guess that gap soliton

would also exist in the now considering supersolid system. Next, we try to find such supersolid gap soliton solutions, and examine their stability, mobility, and collision properties.

III. RESULTS

A. Gap soliton solutions

We find gap soliton by numerically solving the discretized version (the derivative is approximated by second-order central difference) of Eqs. (13), (14), and (15), starting from an initial guessing wave function $\psi_0 = \sum_{i=1,I} A_i \text{sech}[(x - x_i)/\sigma_i]$, where A_i , x_i , σ_i and I are numerically tunable parameters. I determines the number of subwave packets (peaks) of the soliton, x_i , σ_i , A_i are the location, width, and amplitude of each subwave packet. We expect that each subwave packet will fit in a lattice site, thus σ_i is typically set to a value several times smaller than the spatial period of the optical lattice (since the dimensionless optical lattice period is 2π , we typically set σ_i in the range of $0.3 \sim 2$). Parameter A_i is typically set to a value in the range of $0.1 \sim 1$, such that the contact interaction is obvious, but smaller than the depth of optical lattice, and a self-bounded bright soliton solution would be possible. The same typical physical parameters $\Delta_c = -1$, $U = -0.5$, $\kappa = 10$, $\eta = 15$ will be used all along this paper.

In Fig. 3, we show some examples of fundamental soliton wave functions in the first [Figs. 3(a1)–3(c1)] and second [Figs. 3(e1)–3(g1)] energy gaps, together with their corresponding effective optical lattice potentials [Figs. 3(a2)–3(c2); 3(e2)–3(g2)] and energy band structures [Figs. 3(a3)–3(c3); 3(e3)–3(g3)]. When the soliton’s chemical potential lies deep in the energy gap, its wave function is well localized in only one lattice site [Figs. 3(b1) and 3(f1)]. As the chemical potential moves toward the edge of the energy gap, oscillating-decay tails grow out on both sides of the central peak of the wave function. When the chemical potential becomes very close to the gap edge, the tail grows very heavy, see Figs. 3(a1), 3(e1) and 3(c1), 3(g1). Compared with the close to top gap edge case [Figs. 3(c1) and 3(g1)], near the bottom edge of the energy gap, we found that the tail decays much slower, so that the height of the tail peaks becomes almost as high as the central main peak [Figs. 3(a1) and 3(e1)].

The relation between chemical potential and atom number plays an important role in studying gap solitons. It is the basis for classifying gap solitons—a distinct family of gap solitons is usually identified by a continuous N - μ curve [21,26]. For the usual gap solitons in a static optical lattice, this relation is very simple. As the atom number increases, the repulsive interaction leads the chemical potential to grow gradually, i.e., μ is a monotonic increasing function of N [21,26]. Here, the optical lattice potential is built up by pumping the atomic BEC. When the quantum state of BEC changes, the optical lattice potential also changes accordingly. The potential energy will also have an affection on the chemical potential. Therefore, we found that the relationship between N and μ becomes more complex, see Figs. 3(d) and 3(h). For the well-localized soliton with chemical potential deep in the energy gap [Figs. 3(b) and 3(f)], a deep optical lattice is produced (hence the corresponding energy gap is relatively wide), the potential energy makes the chemical potential take

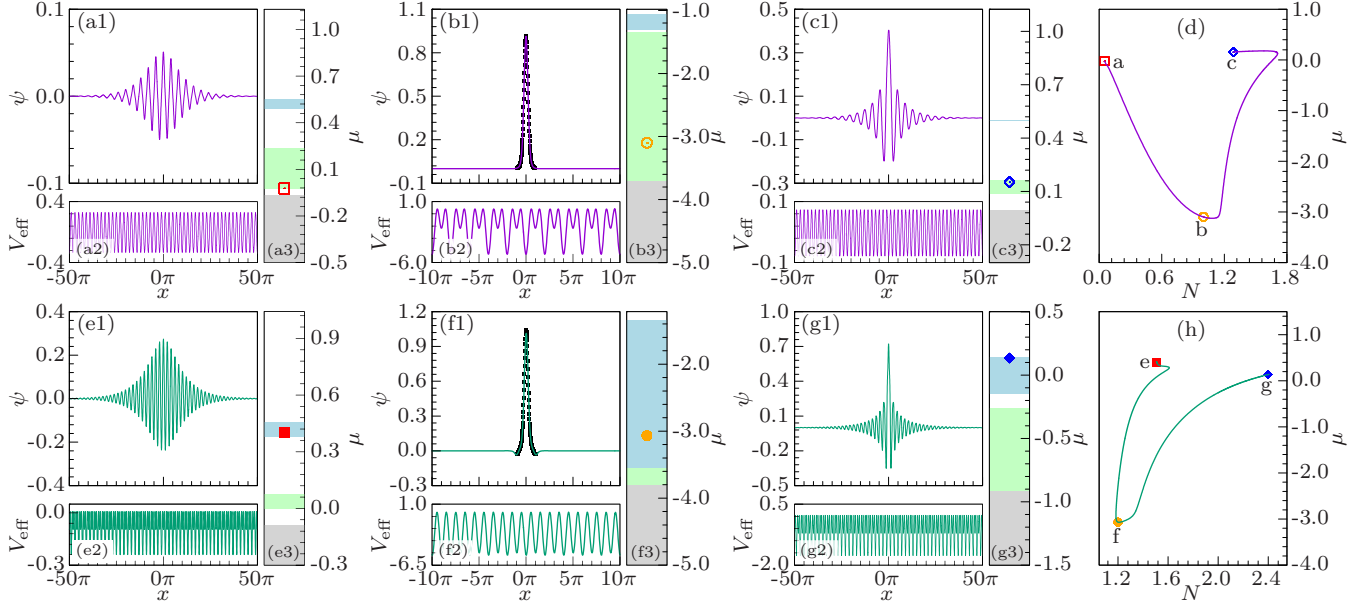


FIG. 3. Fundamental gap solitons in the first (a)–(d) and second (e)–(h) energy gaps. Panels (a1)–(c1) and (e1)–(g1): wave functions $\psi(x)$ of the fundamental gap solitons. In panels (b1), (f1), the black points represent the periodical supersolid states [which have previously been shown in panels (a), (b) of Fig. 2] with the same chemical potential. Panels (a2)–(c2) and (e2)–(g2): corresponding effective optical lattice potentials $V_{\text{eff}}(x)$. Panels (a3)–(c3) and (e3)–(g3): corresponding energy band structures. The gray filled region is the semi-infinite energy gap, the light-green filled region is the first energy gap, the light-blue filled region is the second energy gap, while the unfilled regions are the energy bands (some of the energy bands and gaps are too narrow to be seen very clearly). The colored points mark the chemical potential μ of the corresponding solutions. In panels (a), (e), the chemical potentials lie close to the lower edge of the gap; in panels (b), (f), they lie deep in the gap; and in panels (c), (g), they lie near the upper edge of the gap. Panels (d) and (h): relation between chemical potential μ and atom number N for fundamental gap soliton in the first (d) and second (h) energy gaps. The values of (N, μ) corresponding to solutions of panels (a)–(c) and (e)–(g) are marked on the curve with the colored points which have point style the same as those in panels (a3)–(c3) and (e3)–(g3) and at the same time also explicitly labeled.

a large negative value. Near the edges of the energy gap [Figs. 3(a), 3(e) and 3(c), 3(g)], the soliton wave function extends much wider. According to Eqs. (8)–(15), this will lead to smaller values of $N_{\pm 1, \pm 2}$, consequently a shallower optical lattice (hence the corresponding energy gap becomes narrower) and close to zero chemical potential. Therefore, roughly speaking the N - μ curve takes a “V” shape, as shown in Figs. 3(d) and 3(h). In both these two panels, the right arms of the “V” shapes have a positive dependence of μ on N . This can be understood by the fact that as N increases the repulsive interaction becomes stronger, and at the same time as moves towards the gap edge, the lattice potential also becomes shallower. These two mechanisms both lead to the positive dependence of μ on N . However, in these two panels, the left arms of the “V” shapes have opposite slopes. In Fig. 3(d), as N increases the repulsive interaction energy will increase accordingly. Meanwhile, the induced optical lattice becomes deeper, which leads to a decrease of potential energy. Since the atom number N is small in this regime, it is the decrease of potential energy that plays the main role, thus in total μ has a negative dependence on N . In Fig. 3(h), even for the left arm, the atom number is also considerably large, so this time the repulsive interaction energy dominates the potential energy, and the chemical potential μ will increase with the atom number N . Last, we emphasize that the above discussions are only roughly valid, the dependence of μ on N is in fact very complex, in detail, we also found that the N - μ

curves may anomalously bend near the gap edge [the right end of Fig. 3(d), and the left end of Fig. 3(h)]. This anomalous bent reflects the nonlinear feature of the super-radiant optical lattice, the similar phenomenon also happens for matter-wave solitons in other nonlinear optical lattices [25].

In the second energy gap, other than the fundamental solitons, we also found another family of solitons, see Fig. 4. The wave function of this type of soliton is very similar to the first excited state of a (harmonically) trapped particle. It possesses the odd parity symmetry, at the lattice bottom the wave function takes a zero value, and there are two main peaks (one is positive valued, while the other is negative valued) around this zero point. We distinguish this family of solitons as subfundamental solitons because their wave functions have the same feature as the subfundamental solitons reported in Ref. [26], where gap solitons in a static optical lattice are studied. The (N, μ) data points of this family of solitons form a closed loop, see Fig. 4(g). The chemical potential of this family of solitons can not take values very close to the gap edge, therefore their oscillating-decay tails are always not very heavy. For the same atom number N , the solitons with chemical potential on the upper half part of the N - μ curve [Figs. 4(a)–4(c)] are wider, and at the same time have a heavier oscillating-decay tail, compared to their lower partners [Figs. 4(d)–4(f)].

There also exist many families of high-order gap solitons, which have more than one main peaks. In Fig. 5 (first energy gap) and Fig. 6 (second energy gap), some examples of

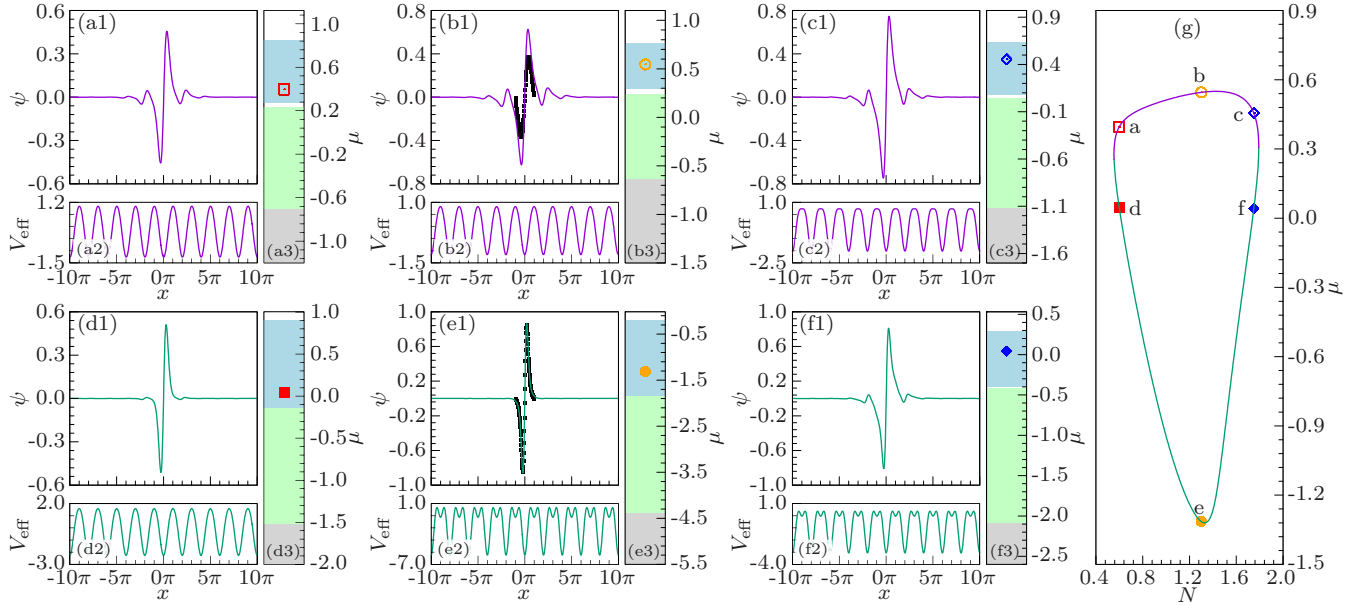


FIG. 4. Subfundamental gap solitons in the second energy gap. Panels (a1)–(f1), (b2)–(f2), (a3)–(f3), and (g) are wave functions, effective optical lattice, energy band structure, and N - μ curve, respectively, and they are plotted the same way as Fig. 3. In panels (b1), (e1), the black points represent the periodical supersolid states [which have previously been shown in Figs. 2(c) and 2(d)] with the same chemical potential. The N - μ curve of this family of soliton is a closed loop, the upper and lower part is plotted with violet and green color, respectively. The solutions of panels (a)–(c) have values of (N, μ) on the upper part of the N - μ loop, while the solutions of panels (d)–(f) have values of (N, μ) on the lower part, as labeled in panel (g).

two, three, and four peaks solutions are shown. Comparing them with the fundamental and subfundamental solitons, it is straightforward to conclude that these high-order solitons can be interpreted as the superposition of fundamental or subfundamental solitons at different lattice sites.

We also compared the spatially periodical supersolid states and the supersolid gap solitons. As shown in Figs. 3(b1) and 3(f1), and Fig. 4(e1), when the gap soliton is well localized in only one lattice site, it has almost the same shape as the periodical supersolid state with the same chemical potential. This indicates that the periodical supersolid state can be recognized as a chain of gap solitons. While for gap soliton with obvious tails around the main peak, its shape will evidently differ from the corresponding periodical solution, this can be seen from Fig. 4(b1). Such similarities and differences between the localized gap soliton and periodical wave have also been reported in the case of static optical lattices [32–35].

B. Stability

The stability of these gap solitons has been checked by numerically evolving the time-dependent Eqs. (5) and (6), with a 5% random perturbation being initially added on the soliton wave function ψ_0 , i.e., $\psi(x, t = 0) = \psi_0[1 + 0.05\xi(x)]$, with $\xi(x)$ being random numbers uniformly distributed in the range of $(-1, 1)$. The corresponding atomic density is $|\psi(x, t = 0)|^2 \approx |\psi_0|^2[1 + 0.1\xi(x)]$, that is the atomic density is perturbed by a magnitude of 10%. However, the perturbation on total atom number is negligible, since the mean value is $\langle \xi(x) \rangle = 0$. We don't explicitly perturb the cavity optical field, it is dynamically determined by the BEC.

Character timescales of the considering system are the dispersion time and cavity loss time. The cavity loss time is estimated by the inverse of loss rate, $\tau_1 = 1/\kappa = 0.1$. The dispersion time is the spreading time of a wave packet due to the kinetic energy term, it is related to the width of the studied wave packet. Here character width of the gap solitons is about

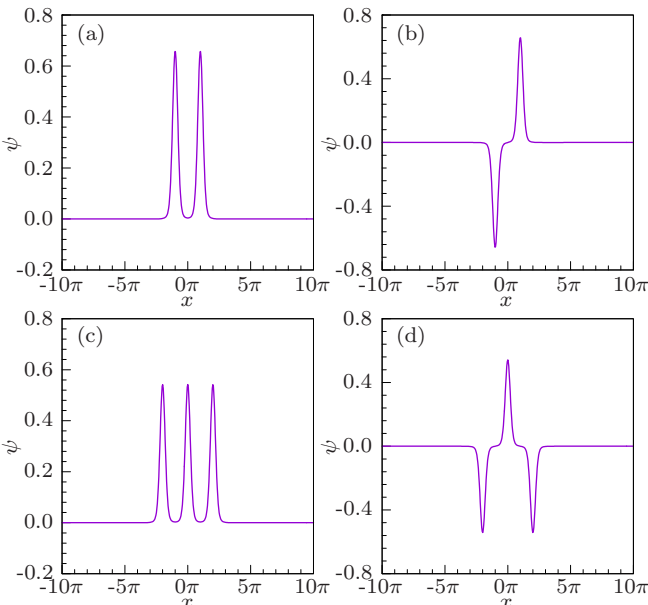


FIG. 5. Examples of high-order gap solitons in the first energy gap. They can be interpreted as combinations of two (a), (b) or three (c), (d) fundamental solitons with the same (a), (c) or opposite (b), (d) phases.

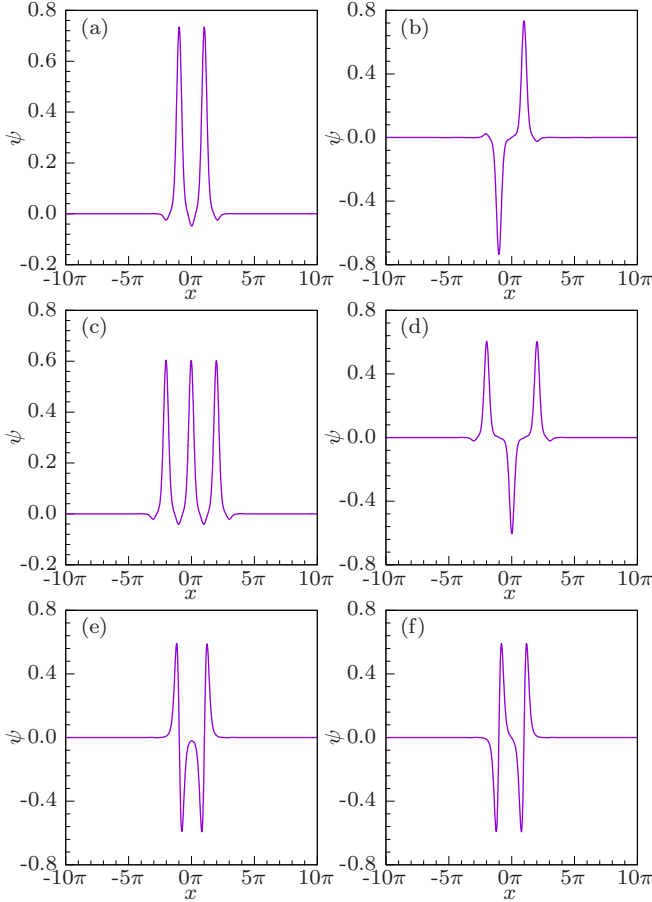


FIG. 6. Examples of high-order gap solitons in the second energy gap. They can be interpreted as combinations of two (a), (b), (e), (f) or three (c), (d) fundamental (a)–(d) or subfundamental (e), (f) solitons with the same or opposite phases.

one lattice length $\sigma \approx \pi$, so that the dispersion time is $\tau_2 = m\sigma^2/\hbar \approx 10$. Thus, for checking the stability, in the numerical simulations, we typically evolve the initial state to a final time $t = 100$ (for the stable solitons) which is much longer than τ_1 and τ_2 , or until the atomic density is substantially different from its initial profile (for the unstable solitons).

The stability results for fundamental solitons in the first energy gap are shown in Figs. 7(a1)–7(g1). In Fig. 7(g1), the overall stability property is summarized on the N - μ curve, with the solid square points referring to stable solitons, while the empty squares for unstable ones. For detailed stability information, in Figs. 7(a1)–7(f1), we show the time evolutions of the atomic density for some typical solitons. In Figs. 7(a1)–7(c1), the solitons can maintain their shape during long time evolution. While, the other ones in Figs. 7(d1)–7(f1) all lose their initial shape very quickly, however in different ways. In Fig. 7(d1), the breathing of atomic density between the main wave packet and the two tail wave packets on its two sides is excited. In Fig. 7(e1), the soliton suffers a severe spatial spreading during the evolution. In Fig. 7(f1), the soliton also suffers an overall spatially spreading, but less severe compared to that in Fig. 7(e1), because the atom density is smaller (therefore, the repulsive interaction is weaker). Another fea-

ture in Fig. 7(f1) is that the wide main wave packet undergoes a sudden shrink at the very beginning time [this is emphasized by an enlarged graph in the top panel of Fig. 8], then the shrunk narrow wave packet can evolve comparatively stable for some time.

The numerical results suggest that the stability of these gap solitons roughly obeys a Vakhitov-Kolokolov (VK) criterion (a negative slope of the N - μ curve, $d\mu/dN < 0$) [31,36–38]. Here, we say “roughly” because of two reasons. First, for the points already on the right-half of the N - μ curve, but still very close to the bottom of the curve, although the VK criterion is invalid, the solitons also can evolve stably for quite a long time. This would result from that the density profile of these solitons changes very slightly during the time evolution, so that the numerical simulation fails to distinguish. Second, at the close to gap edge anomalous bent, some points do have negative slopes, however the solitons are numerically checked to be unstable. This indicates that the VK criterion can not capture the unstable mechanism shown in Fig. 7(f1). We also would like to point out that for the normal repulsive interaction supported BEC gap solitons in static linear optical lattices, their stability obeys the anti-VK criterion by contrast [31,36–38]. This again makes a definite difference between the supersolid gap solitons discussed here and the normal gap solitons in static optical lattices.

The stability results of fundamental solitons in the second energy gap are shown in Figs. 7(a2)–7(g2). In this case, the VK criterion ($d\mu/dN < 0$) is fulfilled in two places—the close to gap edge anomalous bent, and a very narrow range left to the bottom of N - μ curve, see Fig. 7(g2). Numerically, we found that for the anomalous bent, the VK criterion again failed to predict the right stability property, i.e., the solitons are unstable during the time evolution, for an example, see Fig. 7(a2). And around the bottom of N - μ curve, agree with the VK criterion (also roughly, as having been discussed in the previous paragraph), the solitons are checked to be stable, see Fig. 7(d2). All the other points on the N - μ curve are checked to be referring to unstable solitons. On different parts of the N - μ curve, the unstable mechanisms are different. Close to the stable region, the solitons are unstable because of the atomic density breathing, see Figs. 7(c2) and 7(e2). Far away from the stable region, they suffer a spatial spreading, and the larger atom number leads to the severer spreading, this is can be seen from Figs. 7(b2) and 7(f2). These two unstable mechanisms are similar to that in the first energy gap case. At last, at the anomalous bent, we also find a new unstable mechanism. As shown in Fig. 7(a2) and its enlargement in the bottom panel of Fig. 8, this soliton has a very heavy oscillating-decay tail, i.e., the density profile contains many small subwave packets, it is unstable due to the interaction between two neighboring subwave packets.

All the subfundamental gap solitons are numerically found to be unstable, see Fig. 9. Several different unstable mechanisms have been found. First, the two main peaks of a subfundamental soliton can merge into a single peak with a loss of the atoms, see Figs. 9(d) and 9(e). Second, for large atom number subfundamental solitons, the strong repulsive interaction can lead to spatial spreading instability, see Figs. 9(c) and 9(f). Third, in Fig. 9(b), for the soliton on the very top part of N - μ curve, at first it shrinks to another subfundamental

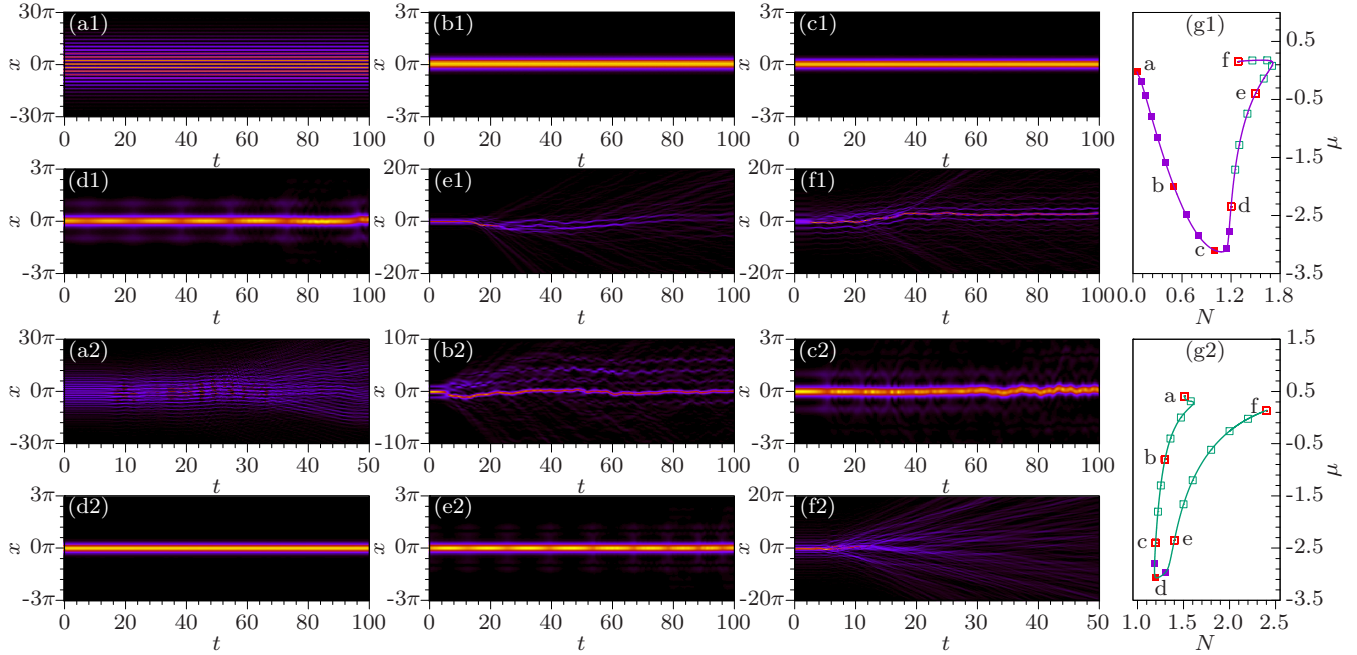


FIG. 7. Stability of fundamental gap solitons in the first (a1–g1) and second (a2–g2) energy gaps. Panels (a1–f1; a2–f2): time evolutions of the atomic density $|\psi(x, t)|^2$ for some example solitons. Panels (g1, g2): stability of the solitons marked on the N - μ curve. The solid square points represent the solitons that are stable during the time evolution, while the empty square points represent the unstable ones. The (N, μ) data points corresponding to panels (a1–f1; a2–f2) are specially plotted with red color, and at the same time also have been explicitly labeled.

soliton with two narrower density peaks (similar to its partner on the lower part of the N - μ curve), then these two narrower peaks merge into a single one again. Last, in Fig. 9(a), we found that at the beginning time the two main peaks of the subfundamental soliton move away from each other, and then spatial oscillations of the wave packets are excited.

Since the high-order solitons can be seen as superposition of fundamental or subfundamental solitons at different lattice sites, we found that they usually have a similar stability feature as their fundamental or subfundamental components, i.e., when the composing solitons are stable, the high-order soliton is also stable and vice versa. For example, solitons (a), (b), (c),

and (d) in Figs. 5 and 6 are found to be stable, while solitons in Figs. 6(e) and 6(f) are unstable.

For comparison, we also examined the stability of normal gap solitons in static periodic potentials whose amplitude and periodicity are the same as the dynamically created optical lattice in ring cavity. We found that in such a static lattice solitons can undergo a stable evolution until the final time of the numerical simulation. So, we think that the instability of the supersolid gap solitons found here is caused by the dynamical property of the optical field.

C. Mobility

In this part, we study mobility of the stable gap solitons. In a ring cavity, lights of the two counterpropagating modes can have independent phases, when their phase difference changes, the optical lattice potential produced by their interference will move. Furthermore, the light field is built up by pumping the BEC. So, it would be reasonable to expect that when the BEC wave packet moves, the optical lattice potential will move accordingly, and will put no extra force on the moving BEC, such that the BEC can move freely. However, this has been demonstrated to be only partially true. More comprehensive studies show that because the light field can not follow the BEC dynamics instantaneously, the optical lattice will fall behind the BEC for a certain distance, and will put a friction force on the BEC, as a result, the BEC will usually undergo a decelerating motion [75,76].

To verify the above discussions, we studied the moving dynamics numerically. We give an initial velocity v_0 to the gap soliton by imprinting a phase factor $\exp[iv_0x]$ on its wave function, then examining the afterward time evolution. The

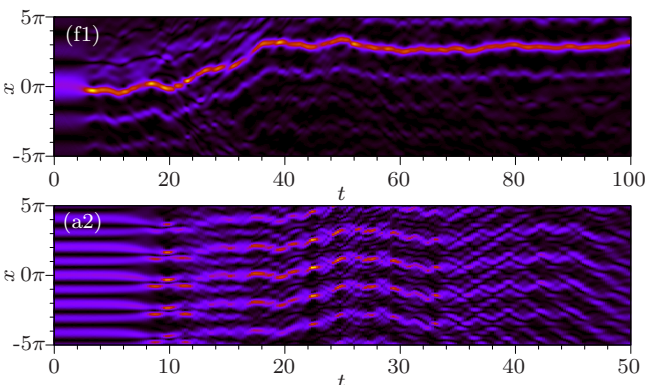


FIG. 8. Enlargements of Figs. 7(f1) and 7(a2). Originally, in Fig. 7, to get the overall information, these two panels are plotted in a wide spatial range. Here, to see the details of interest, they are plotted within a narrow range of $x \in [-5\pi, 5\pi]$.

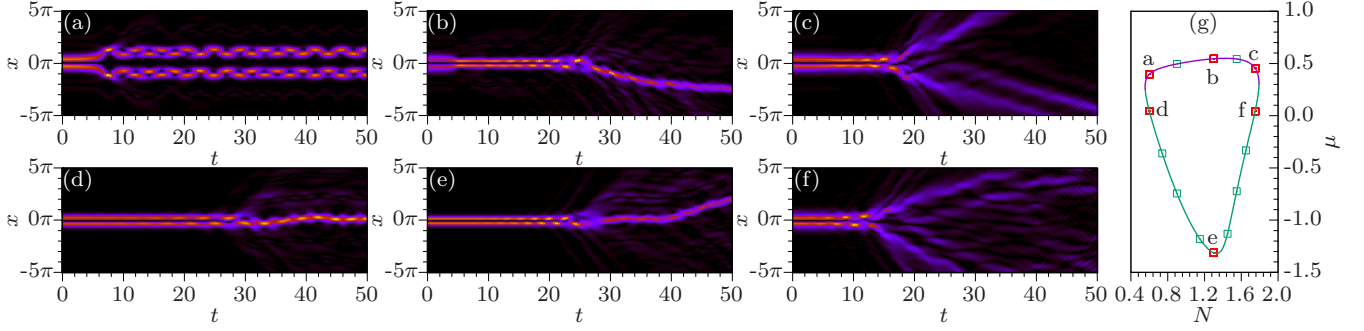


FIG. 9. Stability of the subfundamental gap solitons in the second energy gap. The panels are plotted in a similar way as in Fig. 7. All these subfundamental solitons are unstable.

results are shown in Fig. 10. In Figs. 10(b) and 10(c), for solitons with chemical potential deep in both the first Fig. 10(b) and second Fig. 10(c) energy gaps, we do observe a decelerating motion of the soliton wave packet. In Fig. 10(a), for the soliton with chemical potential near the gap edge, the deceleration is not obvious, it undergoes an almost free motion. This is because in this case the effective optical lattice is very weak [see Fig. 3(a2)], as a result, the friction force is also very small, and its deceleration effect is hard to be obviously observed on the graph.

D. Collision

At last, we show the collision dynamics of two such supersolid gap solitons. In Fig. 11, taking the collisions of two solitons with chemical potential deep in the first energy gap as

an example, the time evolutions of atomic density are plotted for different collision velocities. Although a single such gap soliton is movable (as having been shown in Sec. III C), we found that when the initial colliding velocity is small, two solitons can not approach each other, they only oscillate around their initial locations with a small amplitude, see panel (a). For the medium velocity collision [Figs. 11(b) and 11(c)], the two solitons strongly interact with each other. After some time, the two solitons either break into many small pieces [Fig. 11(b)], or merge into a single wave packet accompanied by a scattering loss of the atoms [Fig. 11(c)]. For the large velocity collision [Fig. 11(d)], the two solitons collide similar to two classical particles, however suffering a spatial

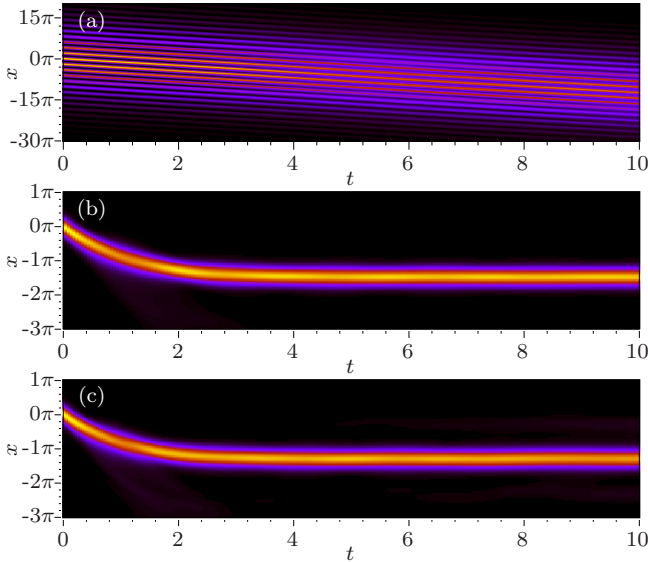


FIG. 10. Mobility of the stable gap solitons. Time evolutions of the atomic density $|\psi(x, t)|^2$ for three different solitons with initial speed $v_0 = 4.0$ are plotted in the three panels. The three solitons are fundamental soliton near the lower edge of the first energy gap (a), deep in the first energy gap (b), and deep in the second energy gap (c), respectively. Their wave functions, effective optical lattice potential, and energy band structures have previously been shown in Figs. 3(a), 3(b), and 3(f).

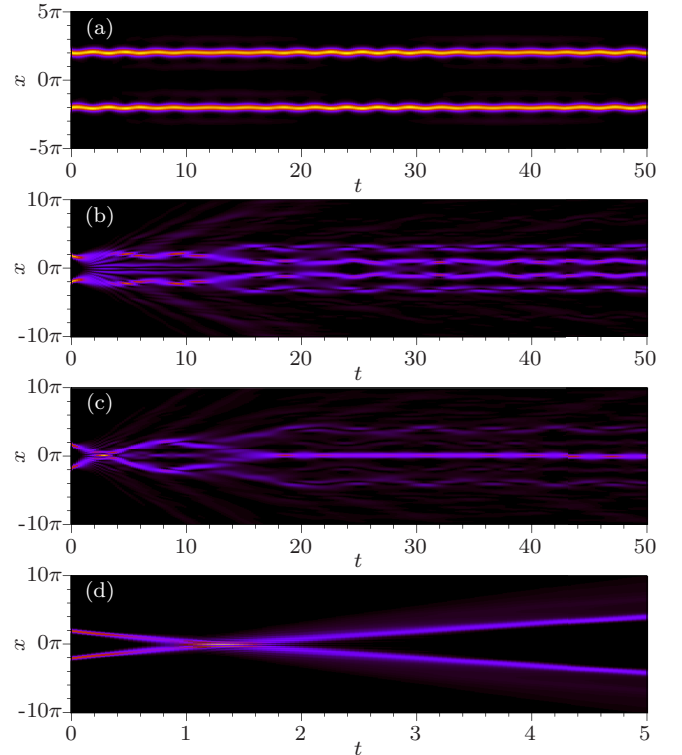


FIG. 11. Collision of two gap solitons (with chemical potential deep in the first energy gap). Time evolutions of the atomic density $|\psi(x, t)|^2$ are plotted. From top to bottom, the initial colliding velocities are set to $v_0 = 0.5$ (a), 2.5 (b), 3.5 (c), and 6.0 (d), respectively.

spreading. Similar collision phenomena have already been observed for nonsoliton wave packets in the same model [77], the explanations also apply here.

Strictly speaking, solitons refers to nonspreading localized wave packets which can interact with other solitons, and emerge from the collision unchanged, except for a phase shift [1]. In this sense, the wave packets in this work would better be called solitary waves. However, in many cases, the collision requirement is often given up, and the term soliton may be used instead of solitary wave [78], here we also follow such a relaxed definition.

IV. SUMMARY

In summary, we predict that there exist supersolid gap solitons in a BEC and optical ring cavity coupling system. We studied the system within the mean-field theory, and numerically found a few families of gap soliton solutions—fundamental gap solitons in both the first and second energy gaps, subfundamental gap solitons in the second energy gap, and high-order gap solitons which consist of several fundamental or subfundamental solitons. The stability of these gap solitons has been checked by numerically simulating the time-dependent mean-field equations. The numerical results suggest that, for the fundamental solitons, their stability roughly obeys the VK criterion, i.e., usually they are stable when their chemical potential μ is negatively dependent on the atom number N ($d\mu/dN < 0$), however, with some ex-

ceptions. All the subfundamental gap solitons are found to be unstable. The high-order gap solitons have similar stability as their fundamental or subfundamental components. For the mobility property, given an initial velocity, these gap solitons usually undergo a decelerating motion due to the friction force from the light fields (the deceleration may be unobvious when friction force is weak). We also studied the two solitons collision dynamics, which are found to be strongly velocity-dependent. For small velocity collision, the two solitons can only oscillate around their initial location with a small amplitude. For medium velocity collision, the two solitons either break into many small pieces, or merge into a single wave packet with a loss of atoms. And the large velocity collision behaves similarly to the collision of two classical particles, except that the two soliton wave packets suffer a spatial spreading.

At last, we note that the BEC and optical ring cavity coupling system has already been realized, and supersolid phase in the system has also been identified [72]. Therefore, the supersolid gap solitons and their dynamical properties reported in this article are ready to be observed experimentally.

ACKNOWLEDGMENTS

The authors acknowledge support from the National Natural Science Foundation of China (Grants No. 11904063, No. 12074120, No. 11847059, and No. 11374003), and the Natural Science Foundation of Shanghai (Grant No. 20ZR1418500).

-
- [1] P. G. Drazin and R. S. Johnson, *Solitons: An Introduction*, 2nd ed. (Cambridge University Press, Cambridge, UK, 1989).
 - [2] P. A. Ruprecht, M. J. Holland, K. Burnett, and M. Edwards, Time-dependent solution of the nonlinear Schrödinger equation for Bose-condensed trapped neutral atoms, *Phys. Rev. A* **51**, 4704 (1995).
 - [3] V. M. Pérez-García, H. Michinel, and H. Herrero, Bose-Einstein solitons in highly asymmetric traps, *Phys. Rev. A* **57**, 3837 (1998).
 - [4] L. Khaykovich, F. Schreck, G. Ferrari, T. Bourdel, J. Cubizolles, L. D. Carr, Y. Castin, and C. Salomon, Formation of a matter-wave bright soliton, *Science* **296**, 1290 (2002).
 - [5] K. E. Strecker, G. B. Partridge, A. G. Truscott, and R. G. Hulet, Formation and propagation of matter-wave soliton trains, *Nature (London)* **417**, 150 (2002).
 - [6] K. E. Strecker, G. B. Partridge, A. G. Truscott, and R. G. Hulet, Bright matter wave solitons in Bose-Einstein condensates, *New J. Phys.* **5**, 73 (2003).
 - [7] S. L. Cornish, S. T. Thompson, and C. E. Wieman, Formation of Bright Matter-Wave Solitons During the Collapse of Attractive Bose-Einstein Condensates, *Phys. Rev. Lett.* **96**, 170401 (2006).
 - [8] T. P. Billam, A. L. Marchant, S. L. Cornish, S. A. Gardiner, and N. G. Parker, Bright solitary matter waves: Formation, stability, and interactions, in *Spontaneous Symmetry Breaking, Self-Trapping, and Josephson Oscillations*, edited by B. A. Malomed (Springer, Berlin, 2013), pp. 403–455.
 - [9] A. D. Jackson, G. M. Kavoulakis, and C. J. Pethick, Solitary waves in clouds of Bose-Einstein condensed atoms, *Phys. Rev. A* **58**, 2417 (1998).
 - [10] R. Dum, J. I. Cirac, M. Lewenstein, and P. Zoller, Creation of Dark Solitons and Vortices in Bose-Einstein Condensates, *Phys. Rev. Lett.* **80**, 2972 (1998).
 - [11] S. Burger, K. Bongs, S. Dettmer, W. Ertmer, K. Sengstock, A. Sanpera, G. V. Shlyapnikov, and M. Lewenstein, Dark Solitons in Bose-Einstein Condensates, *Phys. Rev. Lett.* **83**, 5198 (1999).
 - [12] J. Denschlag, J. E. Simsarian, D. L. Feder, C. W. Clark, L. A. Collins, J. Cubizolles, L. Deng, E. W. Hagley, K. Helmerson, W. P. Reinhardt, S. L. Rolston, B. I. Schneider, and W. D. Phillips, Generating solitons by phase engineering of a Bose-Einstein condensate, *Science* **287**, 97 (2000).
 - [13] B. P. Anderson, P. C. Haljan, C. A. Regal, D. L. Feder, L. A. Collins, C. W. Clark, and E. A. Cornell, Watching Dark Solitons Decay into Vortex Rings in a Bose-Einstein Condensate, *Phys. Rev. Lett.* **86**, 2926 (2001).
 - [14] B. Wu, J. Liu, and Q. Niu, Controlled Generation of Dark Solitons with Phase Imprinting, *Phys. Rev. Lett.* **88**, 034101 (2002).
 - [15] D. J. Frantzeskakis, Dark solitons in atomic Bose-Einstein condensates: From theory to experiments, *J. Phys. A: Math. Theor.* **43**, 213001 (2010).
 - [16] B. A. Malomed, D. Mihalache, F. Wise, and L. Torner, Spatiotemporal optical solitons, *J. Opt. B: Quantum Semiclass. Opt.* **7**, R53 (2005).

- [17] Z. Chen, M. Segev, and D. N. Christodoulides, Optical spatial solitons: Historical overview and recent advances, *Rep. Prog. Phys.* **75**, 086401 (2012).
- [18] Y. Song, X. Shi, C. Wu, D. Tang, and H. Zhang, Recent progress of study on optical solitons in fiber lasers, *Appl. Phys. Rev.* **6**, 021313 (2019).
- [19] G. L. Alfimov, P. G. Kevrekidis, V. V. Konotop, and M. Salerno, Wannier functions analysis of the nonlinear Schrödinger equation with a periodic potential, *Phys. Rev. E* **66**, 046608 (2002).
- [20] P. J. Y. Louis, E. A. Ostrovskaya, C. M. Savage, and Y. S. Kivshar, Bose-Einstein condensates in optical lattices: Band-gap structure and solitons, *Phys. Rev. A* **67**, 013602 (2003).
- [21] N. K. Efremidis and D. N. Christodoulides, Lattice solitons in Bose-Einstein condensates, *Phys. Rev. A* **67**, 063608 (2003).
- [22] B. Eiermann, Th. Anker, M. Albiez, M. Taglieber, P. Treutlein, K.-P. Marzlin, and M. K. Oberthaler, Bright Bose-Einstein Gap Solitons of Atoms with Repulsive Interaction, *Phys. Rev. Lett.* **92**, 230401 (2004).
- [23] B. J. Dabrowska, E. A. Ostrovskaya, and Y. S. Kivshar, Interaction of matter-wave gap solitons in optical lattices, *J. Opt. B: Quantum Semiclass. Opt.* **6**, 423 (2004).
- [24] T. Anker, M. Albiez, R. Gati, S. Hunsmann, B. Eiermann, A. Trombettoni, and M. K. Oberthaler, Nonlinear Self-Trapping of Matter Waves in Periodic Potentials, *Phys. Rev. Lett.* **94**, 020403 (2005).
- [25] H. Sakaguchi and B. A. Malomed, Matter-wave solitons in nonlinear optical lattices, *Phys. Rev. E* **72**, 046610 (2005).
- [26] T. Mayteevarunyoo and B. A. Malomed, Stability limits for gap solitons in a Bose-Einstein condensate trapped in a time-modulated optical lattice, *Phys. Rev. A* **74**, 033616 (2006).
- [27] O. Morsch and M. Oberthaler, Dynamics of Bose-Einstein condensates in optical lattices, *Rev. Mod. Phys.* **78**, 179 (2006).
- [28] H. Sakaguchi and B. A. Malomed, Gap solitons in quasiperiodic optical lattices, *Phys. Rev. E* **74**, 026601 (2006).
- [29] T. Richter, K. Motzek, and F. Kaiser, Long distance stability of gap solitons, *Phys. Rev. E* **75**, 016601 (2007).
- [30] D. L. Wang, X. H. Yan, and W. M. Liu, Localized gap-soliton trains of Bose-Einstein condensates in an optical lattice, *Phys. Rev. E* **78**, 026606 (2008).
- [31] Y. Sivan, G. Fibich, B. Ilan, and M. I. Weinstein, Qualitative and quantitative analysis of stability and instability dynamics of positive lattice solitons, *Phys. Rev. E* **78**, 046602 (2008).
- [32] Y. Zhang and B. Wu, Composition Relation Between Gap Solitons and Bloch Waves in Nonlinear Periodic Systems, *Phys. Rev. Lett.* **102**, 093905 (2009).
- [33] Y. Zhang, Z. Liang, and B. Wu, Gap solitons and Bloch waves in nonlinear periodic systems, *Phys. Rev. A* **80**, 063815 (2009).
- [34] T. J. Alexander and Y. S. Kivshar, Soliton complexes and flat-top nonlinear modes in optical lattices, *Appl. Phys. B* **82**, 203 (2006).
- [35] T. J. Alexander, E. A. Ostrovskaya, and Y. S. Kivshar, Self-Trapped Nonlinear Matter Waves in Periodic Potentials, *Phys. Rev. Lett.* **96**, 040401 (2006).
- [36] H. Sakaguchi and B. A. Malomed, Solitons in combined linear and nonlinear lattice potentials, *Phys. Rev. A* **81**, 013624 (2010).
- [37] Y. V. Kartashov, B. A. Malomed, and L. Torner, Solitons in nonlinear lattices, *Rev. Mod. Phys.* **83**, 247 (2011).
- [38] N. Dror and B. A. Malomed, Stability of two-dimensional gap solitons in periodic potentials: Beyond the fundamental modes, *Phys. Rev. E* **87**, 063203 (2013).
- [39] J. Su, H. Lyu, Y. Chen, and Y. Zhang, Creating moving gap solitons in spin-orbit-coupled Bose-Einstein condensates, *Phys. Rev. A* **104**, 043315 (2021).
- [40] Y. S. Kivshar, W. Krlikowski, and O. A. Chubykalo, Dark solitons in discrete lattices, *Phys. Rev. E* **50**, 5020 (1994).
- [41] S. C. Cheng and T. W. Chen, Dark gap solitons in exciton-polariton condensates in a periodic potential, *Phys. Rev. E* **97**, 032212 (2018).
- [42] L. Zeng and J. Zeng, Gap-type dark localized modes in a Bose-Einstein condensate with optical lattices, *Adv. Photon.* **1**, 046004 (2019).
- [43] J. Li and J. Zeng, Dark matter-wave gap solitons in dense ultracold atoms trapped by a one-dimensional optical lattice, *Phys. Rev. A* **103**, 013320 (2021).
- [44] N. Prokof'ev, What makes a crystal supersolid? *Adv. Phys.* **56**, 381 (2007).
- [45] S. Balibar, The enigma of supersolidity, *Nature (London)* **464**, 176 (2010).
- [46] A. B. Kuklov, N. V. Prokof'ev, and B. V. Svistunov, How solid is supersolid? *Physics* **4**, 109 (2011).
- [47] M. Boninsegni and N. V. Prokof'ev, Supersolids: What and where are they? *Rev. Mod. Phys.* **84**, 759 (2012).
- [48] M. H. W. Chan, R. B. Hallock, and L. Reatto, Overview on solid ^4He and the issue of supersolidity, *J. Low Temp. Phys.* **172**, 317 (2013).
- [49] E. P. Gross, Unified theory of interacting bosons, *Phys. Rev.* **106**, 161 (1957).
- [50] D. J. Thouless, The flow of a dense superfluid, *Ann. Phys.* **52**, 403 (1969).
- [51] A. F. Andreev and I. M. Lifshitz, Quantum theory of defects in crystals, *J. Exp. Theor. Phys.* **29**, 1107 (1969).
- [52] G. V. Chester, Speculations on Bose-Einstein condensation and quantum crystals, *Phys. Rev. A* **2**, 256 (1970).
- [53] A. J. Leggett, Can a solid be "Superfluid"? *Phys. Rev. Lett.* **25**, 1543 (1970).
- [54] E. Kim and M. H. W. Chan, Probable observation of a supersolid helium phase, *Nature (London)* **427**, 225 (2004).
- [55] E. Kim and M. H. W. Chan, Observation of superflow in solid helium, *Science* **305**, 1941 (2004).
- [56] J. Day and J. Beamish, Low-temperature shear modulus changes in solid ^4He and connection to supersolidity, *Nature (London)* **450**, 853 (2007).
- [57] D. Y. Kim and M. H. W. Chan, Absence of Supersolidity in Solid Helium in Porous Vycor Glass, *Phys. Rev. Lett.* **109**, 155301 (2012).
- [58] H. J. Maris, Effect of elasticity on torsional oscillator experiments probing the possible supersolidity of helium, *Phys. Rev. B* **86**, 020502(R) (2012).
- [59] J. R. Li, J. Lee, W. Huang, S. Burchesky, B. Shteynas, F. Ç. Topi, A. O. Jamison, and W. Ketterle, A stripe phase with supersolid properties in spin-orbit-coupled Bose-Einstein condensates, *Nature (London)* **543**, 91 (2017).
- [60] T. M. Bersano, J. Hou, S. Mossman, V. Gokhroo, X.-W. Luo, K. Sun, C. Zhang, and P. Engels, Experimental realization of a long-lived striped Bose-Einstein condensate induced by momentum-space hopping, *Phys. Rev. A* **99**, 051602(R) (2019).

- [61] A. Putra, F. Salces-Cárcoba, Y. Yue, S. Sugawa, and I. B. Spielman, Spatial Coherence of Spin-Orbit-Coupled Bose Gases, *Phys. Rev. Lett.* **124**, 053605 (2020).
- [62] L. Tanzi, E. Lucioni, F. Famà, J. Catani, A. Fioretti, C. Gabbanini, R. N. Bisset, L. Santos, and G. Modugno, Observation of a Dipolar Quantum Gas with Metastable Supersolid Properties, *Phys. Rev. Lett.* **122**, 130405 (2019).
- [63] L. Tanzi, S. M. Rocuzzo, E. Lucioni, F. Famà, A. Fioretti, C. Gabbanini, G. Modugno, A. Recati, and S. Stringari, Supersolid symmetry breaking from compressional oscillations in a dipolar quantum gas, *Nature (London)* **574**, 382 (2019).
- [64] M. Guo, F. Böttcher, J. Hertkorn, J. N. Schmidt, M. Wenzel, H. P. Büchler, T. Langen, and T. Pfau, The low-energy Goldstone mode in a trapped dipolar supersolid, *Nature (London)* **574**, 386 (2019).
- [65] F. Böttcher, J. N. Schmidt, M. Wenzel, J. Hertkorn, M. Guo, T. Langen, and T. Pfau, Transient Supersolid Properties in an Array of Dipolar Quantum Droplets, *Phys. Rev. X* **9**, 011051 (2019).
- [66] L. Chomaz, D. Petter, P. Ilzhöfer, G. Natale, A. Trautmann, C. Politi, G. Durastante, R. M. W. Van Bijnen, A. Patscheider, M. Sohmen, M. J. Mark, and F. Ferlaino, Long-Lived and Transient Supersolid Behaviors in Dipolar Quantum Gases, *Phys. Rev. X* **9**, 021012 (2019).
- [67] M. A. Norcia, C. Politi, L. Klaus, E. Poli, M. Sohmen, M. J. Mark, R. N. Bisset, L. Santos, and F. Ferlaino, Two-dimensional supersolidity in a dipolar quantum gas, *Nature (London)* **596**, 357 (2021).
- [68] M. Sohmen, C. Politi, L. Klaus, L. Chomaz, M. J. Mark, M. A. Norcia, and F. Ferlaino, Birth, Life, and Death of a Dipolar Supersolid, *Phys. Rev. Lett.* **126**, 233401 (2021).
- [69] J. Léonard, A. Morales, P. Zupancic, T. Esslinger, and T. Donner, Supersolid Formation in a quantum gas breaking a continuous translational symmetry, *Nature (London)* **543**, 87 (2017).
- [70] J. Léonard, A. Morales, P. Zupancic, T. Donner, and T. Esslinger, Monitoring and manipulating Higgs and Goldstone modes in a supersolid quantum gas, *Science* **358**, 1415 (2017).
- [71] F. Mivehvar, S. Ostermann, F. Piazza, and H. Ritsch, Driven-dissipative supersolid in a ring cavity, *Phys. Rev. Lett.* **120**, 123601 (2018).
- [72] S. C. Schuster, P. Wolf, S. Ostermann, S. Slama, and C. Zimmermann, Supersolid Properties of a Bose-Einstein Condensate in a Ring Resonator, *Phys. Rev. Lett.* **124**, 143602 (2020).
- [73] L. Salasnich, A. Parola, and L. Reatto, Effective wave equations for the dynamics of cigar-shaped and disk-shaped Bose condensates, *Phys. Rev. A* **65**, 043614 (2002).
- [74] F. Mivehvar, F. Piazza, T. Donner, and H. Ritsch, Cavity QED with quantum gases: New paradigms in many-body physics, *Adv. Phys.* **70**, 1 (2021).
- [75] J. Qin and L. Zhou, Self-trapped atomic matter wave in a ring cavity, *Phys. Rev. A* **102**, 063309 (2020).
- [76] K. Gietka, F. Mivehvar, and H. Ritsch, Supersolid-Based Gravimeter in a Ring Cavity, *Phys. Rev. Lett.* **122**, 190801 (2019).
- [77] J. Qin and L. Zhou, Collision of two self-trapped atomic matter wave packets in an optical ring cavity, *Phys. Rev. E* **104**, 044201 (2021).
- [78] N. Akozbek, *Optical Solitary Waves in a Photonic Band Gap Material* (University of Toronto, 1998).